2024 IEEE International Conference on Robotics and Automation (ICRA 2024)
May 13-17, 2024. Yokohama, Japan

Hybrid Force-Position Control of an Elastic Tendon-Driven Scrubbing Robot (TEDSR)

Noah Harmatz[1], Alina Zahra[1], Amir Abdelmalak[1],

Shivam Purohit[1], Trevor Shin[1], and Aaron D. Mazzeo[1]

[1]Department of Mechanical and Aerospace Engineering, Rutgers University, NJ

***Abstract*—There is a lack of cleaning robots dedicated to the scrubbing of contaminated surfaces. Contaminated surfaces in domestic and industrial settings typically require manual scrubbing which can be costly or hazardous. There is growing demand for automated sanitization systems in hospitals, food-processing plants, and other settings where cleanliness of surfaces is important. To address the opportunity to automate the scrubbing of surfaces, this work focuses on the use of series elastic actuators which can apply consistent trajectories of scrubbing force. Consistent force during scrubbing increases the rate of removal for a contaminant. An elastic robot which has rigid links and low-stiffness joints can perform friction-based cleaning of surfaces with complex geometries while maintaining consistent scrubbing force. This study uses a hybrid force-position control scheme and a low-cost elastic robot to perform scrubbing. This study observes the relationship between joint stiffness in the robot and the disturbance rejection for force-based control during scrubbing.**

I. Introduction

Recent outbreaks of contagious diseases [1], ongoing efforts to contain nosocomial infections [2], and the necessity to maintain sanitary quality of food products [3] have created a demand for new automated sanitization systems in commercial and domestic settings [1], [3]–[5]. New automated sanitization systems can clean contaminated surfaces which are either too difficult, too labor-intensive, or too unsafe for humans to clean. Typical cases of existing automated sanitization systems include vacuum-based floor-cleaning mobile robots [6], [7], spray-cleaning robots [8], [9], and plasma-based cleaning systems [10], [11]. These types of systems perform cleaning with a tool which does not contact the contaminated surface. Vacuum-based cleaning removes loose particles such as dust or sand from a surface, but it does not remove adhesive contaminants such as biofilms [12]. Spray-cleaning systems use jets of liquid to remove adhesive contaminants, but they consume large volumes of water or cleaning chemicals and require drainage systems which are not present in all settings. Plasma-based cleaning inactivates the cells in biofilms to neutralize infectious material, but it does not remove the contaminant from the surface. A new cleaning robot which focuses on the removal of biofilms and other adhesive contaminants from surfaces might use a contact-based method of cleaning.

Scrubbing is a typical form of contact-based cleaning [13]–[15]. Scrubbing uses a friction-based tool to remove contaminating particles from a surface. A kitchen sponge is a common example of a scrubbing tool. As the sponge passes over a surface, it wipes away the contaminating particles [13]. A contaminant with a large adhesive force with a substrate requires a greater amount of mechanical work from the scrubber to achieve complete cleaning. An automated scrubbing system should apply sufficient friction force to a surface to remove the contaminant completely. However, many soft or fragile surfaces may become damaged during excessive scrubbing. There is a growing trend for robots in the field of assistive bathing for humans [16], [17]. In this field, the robot cleans a human patient, particularly an elderly individual or one with limited mobility. Human skin is delicate and may bruise when a scrubber applies too much force. During contact, the robot might apply a gentle touch to not injure the patient.

A scrubbing robot moves a cleaning tool across a contaminated surface, maintaining a friction force in dynamic contact. The robot should maintain a force between its scrubbing tool and the contaminated surface which is large enough to perform effective cleaning but low enough to avoid damaging the surface. A soft robot could sweep a sponge across a surface for gentle contact. Existing designs for soft robots and elastic actuators can perform complex tasks with precise actuation [18]–[20]. Pneumatically-driven elastic actuators can form wheels [21] , airfoils [22], and robotic manipulators [23]. This work suggests an alternative approach with rigid links actuated through elastic tendons. The described elastic robot uses a unique set of rigid links and low-stiffness joints to apply force for effective cleaning and scrubbing with a simple control scheme.

A scrubbing robot requires force feedback to maintain a desired force during cleaning. Force-based measurements are typically noisy and require complex controllers. A hybrid force-position controller is typical for robots which perform

[1] Mazzeo Lab for Machines, Manufacturing, and Mechatronics. Department of Mechanical and Aerospace Engineering. Rutgers, the State University of New Jersey.

979-8-3503-8457-4/24/$31.00 ©2024 IEEE

grinding, polishing, manipulation, or a similar task involving contact between an end tool and a surface [24]–[26]. A hybrid force-position controller adjusts the position of the end effector of the robot during contact to maintain a desired force. Such a controller must account for disturbances such as irregularities on the surface, uncertainty of the position of the end effector relative to the surface, and unmodeled dynamics. An external disturbance will cause deviation from the desired force. Active disturbance rejection control (ADRC) is one strategy which mitigates these disturbances [27], [28]. A typical ADRC consists of a tracking differentiator (TD) and an estimated state observer (ESO). The controller uses feedback from the ESO and input from the TD to track the output y(t) of a system compared to a reference signal r(t). ADRC compensates for any external disturbances and unmodeled dynamics within the system.

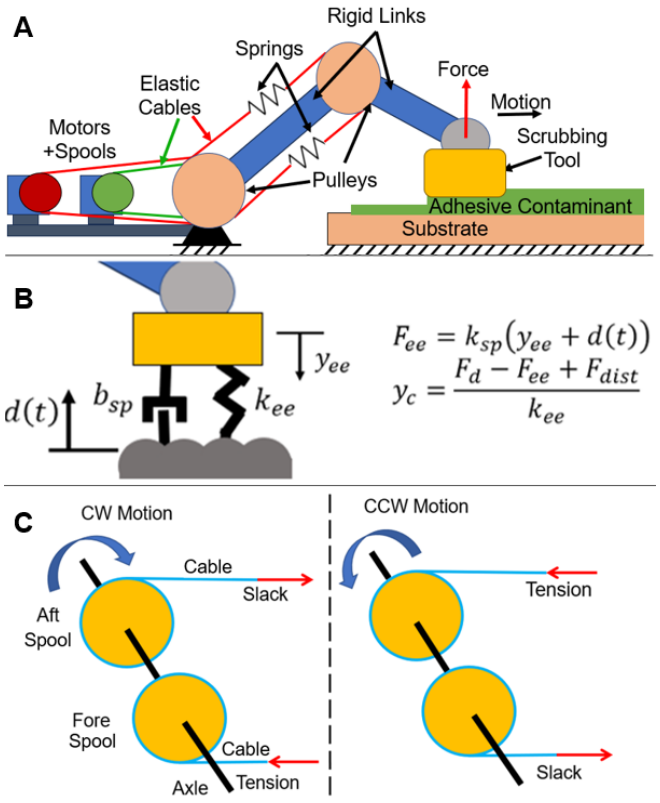

Figure 1. Illustration of a tendon-driven scrubbing robot (TDSR) with series elastic actuators (SEAs). a) An end effector travels across a substrate with an uneven surface. A force sensor measures the normal force which the robot exerts upon the surface. A pair of motors drive spools which actuate two rigid links. b) During scrubbing, a sponge compresses via Hooke's law when the arm presses it against the substrate. The robot uses force feedback to compensate the vertical position of the end effector, maintaining a desired force. c) The cable-driving mechanism consists of two spools on one axle. The aft cable is slung over its spool, and the fore cable is slung under its spool. The direction of rotation for the motor controls tension in both directions of the attached link.

A robot with built-in elasticity and damping could reject external disturbances through passive disturbance rejection (PDR) while using a simpler controller than ADRC. A tendon-driven robot (TDR) arm is a type of robot with built-in elasticity and damping properties [29]. A TDR is a low-inertia alternative to a conventional serial manipulator [30]–[33]. Conventional robot arms often possess a motor in every joint to perform actuation of links. A TDR arm houses all motors inside a torso, and a network of cables connects the motors to anchor points on the links. The tension-driven motion of the cables actuates the links. The elasticity of the cables decreases the stiffness of the joints compared to the rigid joints of conventional robots [32], [34]. Springs put into series with the cables creates a series elastic actuator (SEA) which further reduces the stiffness of the joints [35], [36]. Low-stiffness joints also help reject disturbances in a similar fashion to ADRC with a relatively simple controller [34], [37]. A TDR which uses hybrid force-position control can perform scrubbing while passively rejecting external disturbances. This study considers a TDR which uses proportional-integral-derivative (PID) position control in conjunction with a lead-integral compensator to form a hybrid force-position controller. This novel conjunction of an elastic robot with a simple feedback controller can scrub contaminants effectively from surfaces of various material and geometries. Figure 1 illustrates a tendon-driven scrubbing robot (TDSR).

II. Modeling and Experimental Setup

The disturbance response of a robot follows the model of a mass-spring-damper system at the interface of the robot end effector and the surface. As the robot contacts the surface, a spring-damper response occurs. In the case of a TDSR, the robot compresses the scrubber against the surface. The open-loop disturbance response follows:

$$D(s) = \frac{k\beta(s)}{m_l s^2 + b_l s + k\beta(s)} \quad (1)$$

$$\beta(s) = \frac{x_l(s) - x_o(s)}{x_l(s)} = \frac{m_o s^2 + b_o k}{m_o s^2 + b_o s + k} \quad (2)$$

with mass m, stiffness k, and damping b. Subscript l indicates load, and o indicates output. The disturbance response D(s) is the ratio of the reaction force generated at the interface to the disturbance force. Equation (2) is the transfer function β(s) between the deflection of the scrubber and the position of the link [37]. The system has a natural frequency:

$$\omega_l = \sqrt{\frac{k}{m_l}} \quad (3)$$

As the controller applies an oscillating signal to the system, Soe [37] rewrites:

$$\omega_c = N\omega_l \quad (4)$$

where N is a scalar. Combining (1)-(4) yields:

$$D_{overall}(s) = \frac{\omega_l^2 s^2 + 2\sqrt{2}N\omega_l^3 s + 2N^2\omega^4}{s^4 + 2\sqrt{2}N\omega_l s^3 + (4N^2+1)\omega_l^2 s + 2\sqrt{2}(N^3+N)\omega_l^3 s + (N^4+2N^2)\omega_l^4} \quad (5)$$

Equation 5 shows that the disturbance response depends only on the ratio N. Soe finds that a greater ratio N improves the disturbance rejection of a system with SEAs. In other words, a lower load stiffness causes a greater rejection of disturbance for a given input frequency.

This study uses a three degree-of-freedom (3DoF) robot arm on a rotating base. Two motors actuate the rigid links through elastic tendons. The end effector sits on a passive third joint. The elastic tendons in the first two DoF introduce

a compliance of the upper and lower joints. The compliant joints each have an independent degree of freedom relative to the driving motors. Lens and 2nd author [38] derives the dynamics for a 2DoF elastic serial manipulator which we partition into two domains: the actuator-space and the joint-space. Table 1 summarizes the parameters in the following formulation.

Table 1. Parameters and corresponding symbols for the model of the dynamics of an elastic tendon-driven robot.

Parameter	Symbol
Motor Rotation Position	θ_m
Joint Rotation Position	q_j
Tension	T
Tension Initial	T_0
Radius of Spool	R
Radius of Pulley	r
Jacobian Matrix	J
Stiffness Matrix	K
Damping Matrix	D

The tension in the SEA follows Hooke's Law:

$$T = k\left(R\theta_m - rq_j\right) + T_0 \tag{6}$$

The stretch of the SEA depends on the angular displacement of the motor and the displacement of the joint. Both displacements follow a right-hand-rule convention, with a positive tension resulting from an elongation of the spring. The stiffness matrix K has an off-diagonal term which results from the cable for joint 2 passing over an idler pulley on the same axis as joint 1. The damping matrix D has a similar term.

$$K = \begin{bmatrix} r^2k_1 + R^2k_2 & rRk_2 \\ rRk_2 & R^2k_2 \end{bmatrix} \tag{7}$$

$$D = \begin{bmatrix} r^2d_1 + d_1^2k_2 & rR\,d_2 \\ rR\,d_2 & R^2d_2 \end{bmatrix} \tag{8}$$

k_1 and k_2 refer to the stiffnesses of joints 1 and 2. Likewise, d_1 and d_2 refer to the damping of joints 1 and 2. The torque acting on the actuator-side of the SEA is:

$$\tau_e = K\left(\theta_m - q_j\right) + D\left(\dot{\theta}_m - \dot{q}_j\right) \tag{9}$$

and on the joint-side:

$$\tau_j = J^{-T}\left(K\left(\theta_m - q_j\right) + D\left(\dot{\theta}_m - \dot{q}_j\right)\right) \tag{10}$$

where subscripts e and j refer to the actuator-space and the joint-space. The model includes the motor torque equation:

$$\tau_m = I_m\ddot{\theta}_m + D_m\dot{\theta}_m + \tau_e \tag{11}$$

where I_m and D_m are the inertia and damping of the motor. Rearranging (9)-(11) with the general equation of motion of a serial manipulator to reach torque equations of motion in the joint-space yields:

$$\tau_j = M(q)\ddot{q} + C(q,\dot{q})\dot{q} + D\dot{q} + g(q) \tag{12}$$

$$\tau_j = J^{-T}KJ^{-1}\left(\theta_m - q_j\right) + J^{-T}DJ^{-1}\left(\dot{\theta}_m - \dot{q}_j\right) \tag{13}$$

Equations (11)-(13) form the equations of motion for a tendon-driven serial manipulator.

This study uses a custom-built TDSR, shown in Figure 2, with two links of lightweight aluminum. The robot has two 12V DC gearbox motors, each with a maximum torque of 25 kg-cm. The motors have an internal gear ratio of 270:1. Each motor drives an 8-mm steel shaft. Each shaft houses two spools of 12-mm diameter. Each spool carries a 1.1mm-thick cable of Kevlar with one end fixed to the spool. Each Kevlar cable passes over a series of idler pulleys of 25-mm diameter to attach to an anchor point on one of the aluminum links. Each anchor point is a manually operated tuning peg, such as those found on guitar necks, fixed to the link. Tightening or loosening a knob on each peg fine-tunes the tension in each cable.

One cable on each link actuates clockwise (CW) motion of the link when pulled in tension, and the other cable controls the counterclockwise (CCW) motion as Figure 1c illustrates. Each motor controls the two directions of rotation of its link through the tension in both cables. This study introduces the elastic tendon-driven scrubbing robot (TEDSR) which can perform scrubbing of adhesive stains on common surfaces. Each motor connects to an L298N motor driver for power, both powered by DC power supply. A National Instruments (NI) myRIO-1900 controls the motors using a custom LabVIEW program. The robot arm sits upon a custom-manufactured rotating base of additively manufactured polylactic acid (PLA). An S51 micro servo motor drives a planetary gear system within the base to rotate the arm. The two-link arm moves the scrubber in the x-y plane, and the rotation permits scrubbing in the lateral z- direction.

The wrist of the robot is a passive joint with a custom-built end-effector mount. The mount consists of three components of additively manufactured PLA. The assembly of the three components permits a pin-joint attachment of the housing to an 8mm axle at the distal end of the second link. The housing contains a slot for a force-sensing load cell. This study uses 5kg compression mini button load cell. The load cell bolts into the top half of the housing. The geometry of the top half of the housing permits the bottom half to slide into a pair of small rails. The rails hold the housing together but do not transmit force through to the top half. This geometry permits all normal force acting on the housing to transfer through the load cell. The housing permits the attachment of a Mister Clean Magic Eraser scrubbing tool to the underside. The scrubber has a contact area of 60mm x 119 mm. The load cell measures the normal force which the scrubber exerts upon a contacted surface. The load cell passes the force data to the myRIO, and the LabVIEW program records the data as the end effector moves across a surface. TEDSR uses the scrubbing tool to perform scrubbing on contaminated surfaces.

During scrubbing, the sponge compresses between the end effector (EE) and the substrate by Hooke's Law:

$$F_{ee}(t) = k\left(y_{ee}(t) - d(t)\right) \tag{14}$$

where k is the stiffness of the sponge, $y_{ee}(t)$ is the vertical position of the sponge, and d(t) is the height of the surface. This study compensates $y_{ee}(t)$ of the sponge to maintain a desired contact force. Rewriting (14) in terms of y(t) yields:

$$y_c = \frac{F_d - F_{ee} + F_{dist}}{k_{ee}} \tag{15}$$

where y_c is the compensated position of the sponge, F_d is the desired force, and F_{dist} is any external disturbance. The controller adjusts the desired height y_c, illustrated in Figure 1.

Many scrubbing applications occur on flat surfaces such as floors, windows, and countertops. Other scrubbing

applications occur on surfaces with curved or irregular geometries such as sinks, stovetops, and toilets. A scrubbing

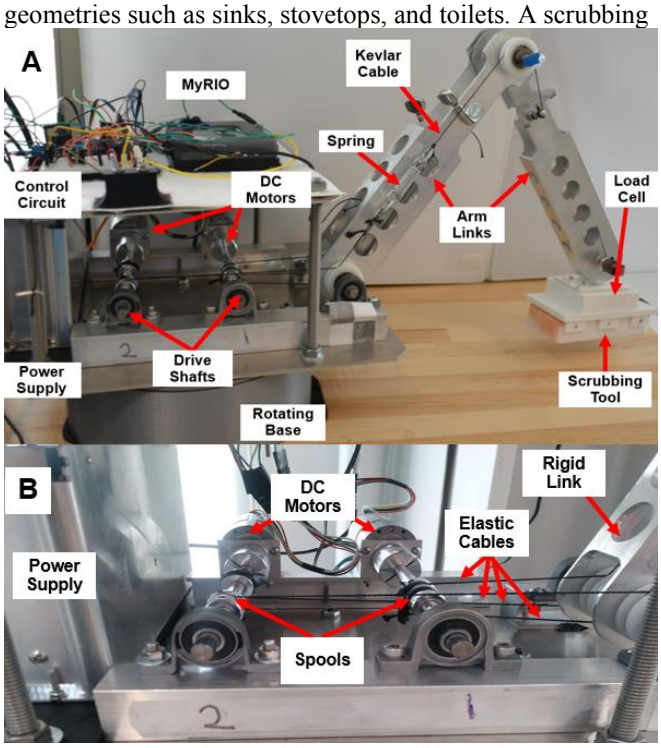

Figure 2. Experimental setup with uneven scrubbing surface. a) A custom-built 2DoF robot arm sits atop a rotary base. Two motors actuate two rigid links through the tension control of series elastic actuators (SEAs). The SEAs each consist of a tension spring in series with a Kevlar cable. A passive joint at the end of the arm contains an attachment point for a scrubbing tool and a custom-built rolling probe. A force-sensing load cell sits inside the end effector to measure the force exerted by the robot on the surface. the end effector scrubs back and forth across the surface. A 3D printed sinusoidal track provides an uneven surface with known geometry for testing of disturbance rejection. b) A close-up image of the motor block. Two DC motors sit mounted on parallel bars to support the driving torques acting through the elastic cables on the rigid links.

robot should be able to clean both flat and curved surfaces. This study considers two types of surfaces for testing the robot: a flat ceramic tile and a plastic mannequin body. The curved geometry of the mannequin creates disturbances in the force profile as the robot moves the end effector along the track. The robot must adjust its vertical position to maintain a constant force while moving along the surface, as Figure 1b illustrates.

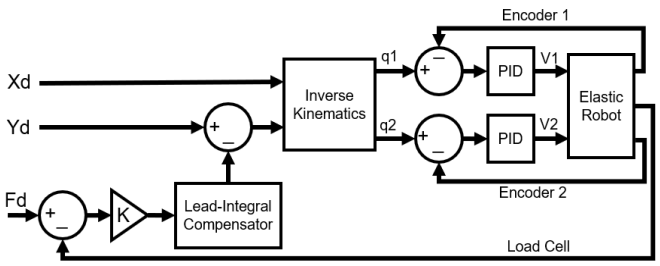

Figure 3. Implemented control scheme for hybrid force-position control. The controller accepts desired position (X_d and Y_d) and a desired force (F_d). An inverse kinematics solver outputs desired joint angles (q_1 and q_2). A position-control loop uses PID-based error control to achieve desired joint positions of the robotic links to reach a desired end-effector position in space. The PID controllers output voltages (V_1 and V_2) to the DC motors on the robot. Encoders on the robot outputs the position of the motors as feedback for the PID blocks. A lead-integral compensator computes the error between F_d and feedback from a load cell on the robot to adjust the vertical position of the end effector with respect to a surface.

This study uses a custom hybrid force-position program in LabVIEW to control the robot. The program uses PID position control of two motors to reach a desired pose of the robot. An inverse kinematics program uses a desired end effector position to compute the desired pose. Encoders provide feedback for the position of the two motors. The controller in Figure 3 uses the motor position, the transmission ratio of the spool-pulley system, and the dynamics of the elastic robot to estimate the state of the joint angles. A lead-integral compensator uses feedback from the load cell to adjust the end effector vertical position to maintain a desired force during contact. The compensator applies (15) to adjust y_d and maintain the desired force.

III. Experimental Results

A loading-unloading vibration test determines the stiffness of the two joints. The robot rests in a neutral orientation for scrubbing without position control. A human user displaces one link manually by a small angle and then releases. A video camera captures the resulting oscillation of the link. The user repeats this procedure for the other link. Figure 4 illustrates the oscillations and summarizes the results. This study finds the stiffness of a joint by:

$$k = \frac{4\pi^2 I}{T^2} \tag{16}$$

where T is the period of oscillation and I is the moment of inertia of the link. The perturbation of link 1 includes the inertia of both link 1 and link 2 (0.46 kg). A custom image-processing algorithm accepts video data of the response. The algorithm calculates the frequencies of oscillation. This study uses video data to capture the oscillations rather than a pair of IMU sensors, as the addition of sensors would increase the complexity of the robot design.

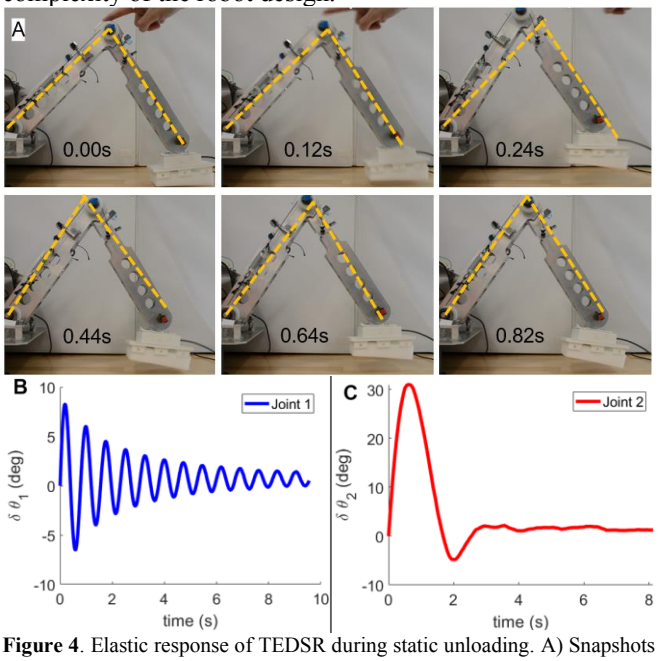

Figure 4. Elastic response of TEDSR during static unloading. A) Snapshots of the robot after release from static loading. The cables hold tension during static loading and cause oscillations about an equilibrium position when

released from a static loading. Dashed yellow lines indicate the position of the links in the previous snapshot to highlight the motion of the arm. B-C) The angular response upon release of loading for link 1 (B) and link 2 (C). We use the inertia of the links and the frequency of oscillation to calculate the stiffness of each joint. Joints 1 and 2 have stiffnesses of 32.8 and 28.7 N-m/rad, respectively. The joints have damping values of 0.04 and 0.17 N-m/rad-s, respectively.

The frequencies of oscillation for links 1 and 2 are 1.34 Hz and 1.78 Hz, respectively. These frequencies and (16) yield stiffness values of 32.8 N-m/rad and 28.7 N-m/rad for the two joints.

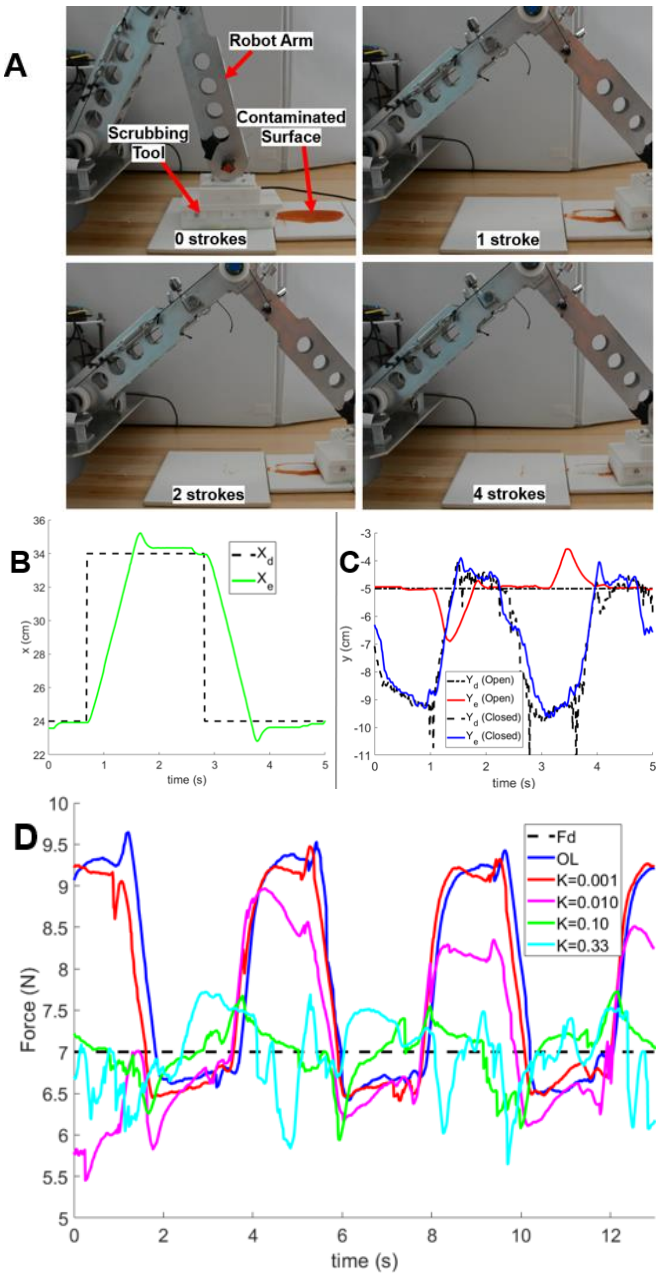

Figure 5. a) The robot scrubs tomato sauce from a flat tile surface over multiple strokes. Each stroke removes a portion of the remaining stain. The controller adjusts the vertical position of the scrubber to maintain a desired force during scrubbing. b) The desired (X_d) and estimated (X_e) x-positions of the end effector over a 5-second span of scrubbing. The x-position is the same for open- and closed-loop force control. c) The desired (Y_d) and estimated (Y_e) y-positions for open- and closed-loop force control. Closed-loop force control adjusts Y_e to maintain a desired force. d) Force data for the robot scrubbing across a flat countertop. Each line represents a different gain for the force compensator. The controller sets a desired force F_d (in this case, 7 N) for the robot to maintain. In the uncontrolled case (OL) with pure position control, the robot has a deviation of up to 2.6 N or 37% error. An increasing gain K reduces the deviation from the desired force. A gain of 0.10 yields a deviation within 1Dof the desired value, or 14% error.

This study considers the effectiveness of scrubbing tomato sauce from a tile surface. The robot arm uses a Mister Clean Magic Eraser melamine scrubbing tool to perform scrubbing. The arm passes the scrubber over the contaminated tile surface as illustrated in Figure 5a and 6a. The scrubber strokes back and forth across the stain five times. Each successive stroke removes a portion of the remaining stain. A camera records a top-down view of the tile before and after scrubbing, as illustrated in Figure 6b. A custom image-processing algorithm measures the amount of tomato sauce on the tile based on red pigment. This study defines cleaning effectiveness as the ratio of the amount of red pigment removed to the initial amount of pigment.

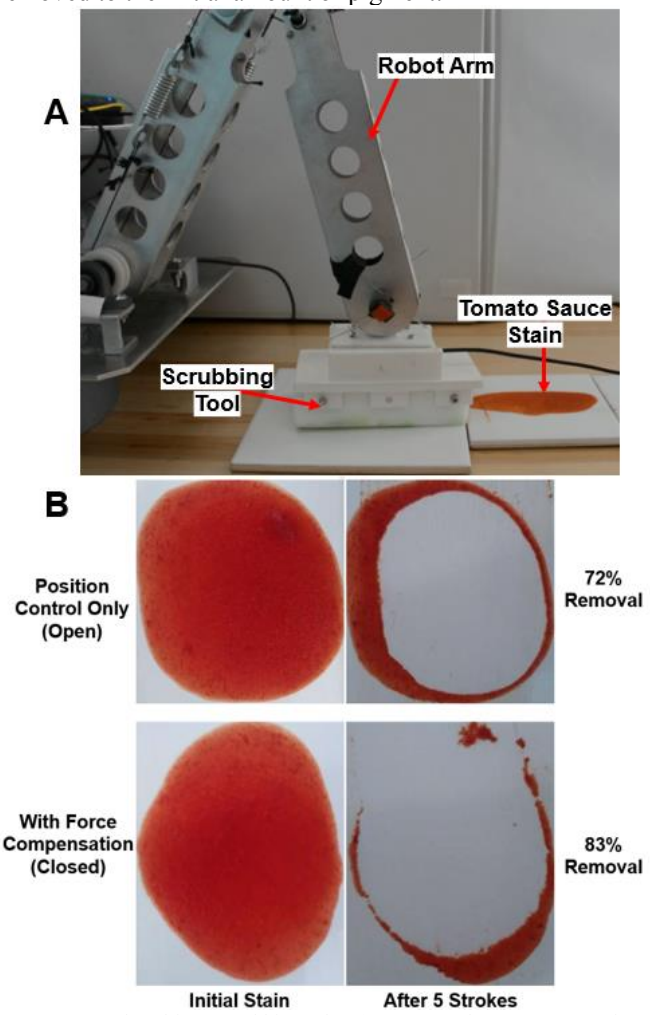

Figure 6. Tendon-driven scrubbing robot (TDSR) scrubs tomato sauce from a tile surface using pure position control (open loop) and using hybrid force-position control (closed loop). a) A custom-fitted end effector allows the attachment of a melamine scrubbing sponge. The robot moves the sponge across a tile surface contaminated with spilt tomato sauce. b) A custom image-processing algorithm measures the amount of tomato sauce remaining after 5 strokes with both control styles. Closed-loop force control increases the effectiveness of scrubbing by 11% compared to pure position control.

We first focus on the removal of stain from a control area, and future tests could measure the amount of mass removed from the surface. With a pure position-control approach, the scrubber removes 72% of the contaminant. The addition of force-based feedback to maintain a downward force of 7 N, the scrubber removes 83% of the contaminant. The addition of force compensation improves the cleaning effectiveness by an average of 11% over five trials.

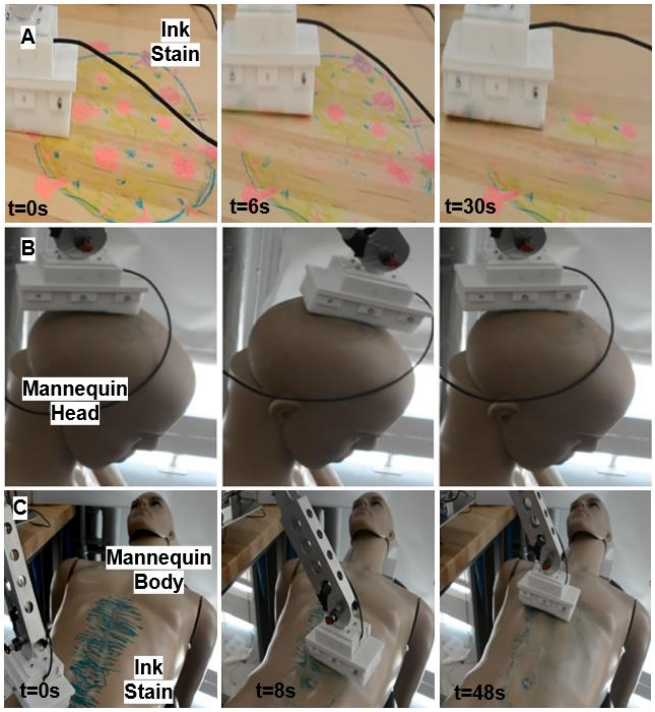

Figure 7. Scrubbing robot removing ink stain from contaminated surfaces. a) TEDSR scrubs an ink stain one foot in diameter from a flat countertop. b) TEDSR scrubs the head of a mannequin. The sponge passes over the curved surface to remove blue ink. c) TEDSR scrubs over the mannequin body's surface to remove ink. The process takes less than one minute. The compliant sponge and the force controller allow the robot to track across the uneven surface, removing the stain from cervices along the surface which would otherwise be difficult to clean.

IV. Discussion

Decreasing the stiffness of robotic joints reduces the required complexity of a controller to reject disturbances in a scrubbing application. A conventional robot with large joint stiffnesses has a low fidelity of force measurement. The noise in force measurements which occur during scrubbing contact would require the motors to adjust the position of the scrubber at a high frequency. An elastic robot reduces the noise in force measurements during scrubbing. The elasticity in the SEAs reduces the stiffness of the joints compared to a conventional robot. The elastic robot has a soft-like response during contact with a surface. The softness of the robot depends on the stiffness of the springs in series with the Kevlar cables. An elastic robot with even lower joint stiffnesses would have a softer touch, but the cables must then stretch a greater amount to achieve a desired change in pose. The design of an elastic scrubbing robot should find a nominal range of joint stiffnesses to be capable of effective scrubbing while maintaining the softness of contact. This study uses a design with interchangeable springs to tune the stiffness of the joints. Changing out the springs can only occur when the robot is not moving. A future iteration of this design would add a new mechanism to actively tune the stiffness of the joints during scrubbing.

Future iterations of this work could perform scrubbing on soft surfaces. The forces involved in typical scrubbing applications are unlikely to damage a ceramic tile countertop, but surfaces such as produce skin or rubber mats with low material hardness could undergo damage under heavy loads. A scrubbing robot must exert enough force upon a surface to clean it but not too great a force that it damages the surface it is cleaning.

There is ongoing work to implement a computer vision algorithm which can identify the surface TEDSR is cleaning and the type of stain it is removing. An RGB-D camera records image data which detects the red pigment of a tomato-based stain. The next steps involve programming the robot to scrub a surface with red pigment until the pigment is gone. An advanced algorithm will seek a variety of stains based on image data. Scrubbing dirt from a fragile or soft surface such as glass countertop requires precise force control. Further, scrubbing grime from human skin during a sponge bath requires a high level of safety to prevent discomfort or injury. TEDSR could use verbal or non-verbal feedback from a human to ensure a safe procedure.

V. Conclusion

This study introduces an elastic tendon-driven scrubbing robot (TEDSR) capable of removing adhesive stains from contaminated surfaces. The low-stiffness joints of TEDSR permit a relatively simple hybrid force-position controller to move a scrubbing tool across the contaminated surface. Force feedback from a load cell adjusts the position of the scrubber relative to the normal of the surface. A K-value for the force compensator between 0.10 and 0.33 rejects disturbances while scrubbing along a surface, yielding 14% error from a desired force. Further tuning of the lead-integral controller and additional damping to the elastic joints can improve the disturbance rejection. TEDSR can remove stains such as ink and tomato sauce from contaminated surfaces. The robot can remove stronger stains with longer duration of cleaning or with the addition of a cleaning fluid such as water. TEDSR can remove adhesive stains from surfaces such as floors, tables, walls, toilets, sinks and human patients. An elastic scrubbing robot can operate near humans in hospitals, schools, factories, laboratories, and any setting where surfaces need cleaning.

Acknowledgment

The authors acknowledge support from National Science Foundation Award Number 2021628. N.H. and A.D.M. designed the research. N.H., S.P., T.S., and A.Z. constructed the robot platform. N.H., A.A., and A.Z. performed the research and data collection. N.H., A.Z., and A.D.M. analyzed the data. N.H., A.Z., and A.D.M wrote the paper.

REFERENCES

[1] M. H. Khan and H. Yadav, "Sanitization During and After COVID-19 Pandemic: A Short Review," *Trans. Indian Natl. Acad. Eng.*, vol. 5, no. 4, pp. 617–627, Dec. 2020, doi: 10.1007/s41403-020-00177-9.

[2] G. E. Morfill, T. Shimizu, B. Steffes, and H.-U. Schmidt, "Nosocomial infections—a new approach towards preventive medicine using plasmas," *New J. Phys.*, vol. 11, no. 11, p. 115019, Nov. 2009, doi: 10.1088/1367-2630/11/11/115019.

[3] Q. Wang *et al.*, "Cold plasma from flexible and conformable paper-based electrodes for fresh produce sanitation: Evaluation of microbial inactivation and quality changes," *Food Control*, vol. 137, p. 108915, Jul. 2022, doi: 10.1016/j.foodcont.2022.108915.

[4] Z. Nakat and C. Bou-Mitri, "COVID-19 and the food industry: Readiness assessment," *Food Control*, vol. 121, p. 107661, Mar. 2021, doi: 10.1016/j.foodcont.2020.107661.

[5] J. Xie, Q. Chen, P. Suresh, S. Roy, J. F. White, and A. D. Mazzeo, "Paper-based plasma sanitizers," *Proc. Natl. Acad. Sci.*, vol. 114, no. 20, pp. 5119–5124, May 2017, doi: 10.1073/pnas.1621203114.

[6] V. Prabakaran, M. R. Elara, T. Pathmakumar, and S. Nansai, "Floor cleaning robot with reconfigurable mechanism," *Autom. Constr.*, vol. 91, pp. 155–165, Jul. 2018, doi: 10.1016/j.autcon.2018.03.015.

[7] T. B. Asafa, T. M. Afonja, E. A. Olaniyan, and H. O. Alade, "Development of a vacuum cleaner robot," *Alex. Eng. J.*, vol. 57, no. 4, pp. 2911–2920, Dec. 2018, doi: 10.1016/j.aej.2018.07.005.

[8] L. A. Langøyli Giske, E. Bjørlykhaug, T. Løvdal, and O. J. Mork, "Experimental study of effectiveness of robotic cleaning for fish-processing plants," *Food Control*, vol. 100, pp. 269–277, Jun. 2019, doi: 10.1016/j.foodcont.2019.01.029.

[9] A. S. A. Ghafar, S. S. H. Hajjaj, K. R. Gsangaya, M. T. H. Sultan, M. F. Mail, and L. S. Hua, "Design and development of a robot for spraying fertilizers and pesticides for agriculture," *Mater. Today Proc.*, Apr. 2021, doi: 10.1016/j.matpr.2021.03.174.

[10] H. A. Aboubakr, F. Sampedro Parra, J. Collins, P. Bruggeman, and S. M. Goyal, "In situ inactivation of human norovirus GII.4 by cold plasma: Ethidium monoazide (EMA)-coupled RT-qPCR underestimates virus reduction and fecal material suppresses inactivation," *Food Microbiol.*, vol. 85, p. 103307, Feb. 2020, doi: 10.1016/j.fm.2019.103307.

[11] T. N. Das, V. Perayya, and P. G. Abichandani, "Design of Cold Plasma Flexible Brush and Evaluation of Its Oxidizing Plume," *IEEE Trans. Plasma Sci.*, vol. 46, no. 7, pp. 2536–2545, Jul. 2018, doi: 10.1109/TPS.2018.2803823.

[12] S. Achinas, N. Charalampogiannis, and G. J. W. Euverink, "A Brief Recap of Microbial Adhesion and Biofilms," *Appl. Sci.*, vol. 9, no. 14, p. 2801, 2019, doi: http://dx.doi.org/10.3390/app9142801.

[13] Y. Huang, D. Guo, X. Lu, and J. Luo, "Modeling of particle removal processes in brush scrubber cleaning," *Wear*, vol. 273, no. 1, pp. 105–110, Nov. 2011, doi: 10.1016/j.wear.2011.06.022.

[14] K. Xu *et al.*, "Fundamental study of the removal mechanisms of nano-sized particles using brush scrubber cleaning," *J. Vac. Sci. Technol. B Microelectron. Nanometer Struct. Process. Meas. Phenom.*, vol. 23, no. 5, pp. 2160–2175, Sep. 2005, doi: 10.1116/1.2052713.

[15] L. A. Langøyli Giske, L. H. Lindstad, T. Løvdal, and O. J. Mork, "Design of fish processing equipment: exploring cleaning brush performance and material properties to minimize biofilm deposits," *Procedia CIRP*, vol. 91, pp. 140–145, Jan. 2020, doi: 10.1016/j.procir.2020.02.159.

[16] A. Zlatintsi *et al.*, "I-Support: A robotic platform of an assistive bathing robot for the elderly population," *Robot. Auton. Syst.*, vol. 126, p. 103451, Apr. 2020, doi: 10.1016/j.robot.2020.103451.

[17] Chih-Hung King, T. L. Chen, A. Jain, and C. C. Kemp, "Towards an assistive robot that autonomously performs bed baths for patient hygiene," in *2010 IEEE/RSJ International Conference on Intelligent Robots and Systems*, Taipei: IEEE, Oct. 2010, pp. 319–324. doi: 10.1109/IROS.2010.5649101.

[18] A. Chen, R. Yin, L. Cao, C. Yuan, H. K. Ding, and W. J. Zhang, "Soft robotics: Definition and research issues," in *2017 24th International Conference on Mechatronics and Machine Vision in Practice (M2VIP)*, Auckland: IEEE, Nov. 2017, pp. 366–370. doi: 10.1109/M2VIP.2017.8267170.

[19] C. Lee, M. Kim, Y. Kim, N. Hong, S. Ryu, and S. Kim, "Soft robot review," *Int. J. Control Autom. Syst.*, vol. 15, Jan. 2017, doi: 10.1007/s12555-016-0462-3.

[20] F. Ilievski, A. D. Mazzeo, R. F. Shepherd, X. Chen, and G. M. Whitesides, "Soft Robotics for Chemists," *Angew. Chem. Int. Ed.*, vol. 50, no. 8, pp. 1890–1895, 2011, doi: 10.1002/anie.201006464.

[21] X. Gong *et al.*, "Rotary Actuators Based on Pneumatically Driven Elastomeric Structures," *Adv. Mater.*, vol. 28, no. 34, pp. 7533–7538, 2016, doi: 10.1002/adma.201600660.

[22] J. Xie, J. B. McGovern, R. Patel, W. Kim, S. Dutt, and A. D. Mazzeo, "Elastomeric Actuators on Airfoils for Aerodynamic Control of Lift and Drag," *Adv. Eng. Mater.*, vol. 17, no. 7, pp. 951–960, 2015, doi: 10.1002/adem.201500036.

[23] X. Zou *et al.*, "Paper-Based Robotics with Stackable Pneumatic Actuators," *Soft Robot.*, vol. 9, no. 3, pp. 542–551, Jun. 2022, doi: 10.1089/soro.2021.0002.

[24] D. Jeon and M. Tomizuka, "Learning hybrid force and position control of robot manipulators," *IEEE Trans. Robot. Autom.*, vol. 9, no. 4, pp. 423–431, Aug. 1993, doi: 10.1109/70.246053.

[25] Y. Dong, T. Ren, K. Hu, D. Wu, and K. Chen, "Contact force detection and control for robotic polishing based on joint torque sensors," *Int. J. Adv. Manuf. Technol.*, vol. 107, no. 5, pp. 2745–2756, Mar. 2020, doi: 10.1007/s00170-020-05162-8.

[26] "Model Predictive Force Control in Grinding based on a Lightweight Robot," *IFAC-Pap.*, vol. 52, no. 13, pp. 1779–1784, Jan. 2019, doi: 10.1016/j.ifacol.2019.11.459.

[27] R. Fareh, S. Khadraoui, M. Y. Abdallah, M. Baziyad, and M. Bettayeb, "Active disturbance rejection control for robotic systems: A review," *Mechatronics*, vol. 80, p. 102671, Dec. 2021, doi: 10.1016/j.mechatronics.2021.102671.

[28] O. S. Khairallah, "Robotics Control Using Active Disturbance Rejection Control".

[29] K. Choi *et al.*, "A hybrid dynamic model for the AMBIDEX tendon-driven manipulator," *Mechatronics*, vol. 69, p. 102398, Aug. 2020, doi: 10.1016/j.mechatronics.2020.102398.

[30] B. Okur, O. Aksoy, E. Zergeroglu, and E. Tatlicioglu, "Nonlinear Robust Control of Tendon–Driven Robot Manipulators," *J. Intell. Robot. Syst.*, vol. 80, no. 1, pp. 3–14, Oct. 2015, doi: 10.1007/s10846-014-0141-7.

[31] T. Takuma, "Design of Tendon-Driven Mechanism Using Geometrical Condition," *Actuators*, vol. 9, no. 3, Art. no. 3, Sep. 2020, doi: 10.3390/act9030048.

[32] T. Lens and O. Von Stryk, "Investigation of Safety in Human-Robot-Interaction for a Series Elastic, Tendon-Driven Robot Arm," presented at the Proceedings of the ... IEEE/RSJ International Conference on Intelligent Robots and Systems. IEEE/RSJ International Conference on Intelligent Robots and Systems, Oct. 2012, pp. 411–422. doi: 10.1007/978-3-642-17319-6_38.

[33] M. Ho and J. P. Desai, "Towards the Development of a Tendon-Driven Neurosurgical Robot," in *ASME 2011 Dynamic Systems and Control Conference and Bath/ASME Symposium on Fluid Power and Motion Control, Volume 2*, Arlington, Virginia, USA: ASMEDC, Jan. 2011, pp. 795–797. doi: 10.1115/DSCC2011-6075.

[34] A. Hiraoka and T. Murakami, "An Approach of Load-Side Disturbance Rejection Control for Series Elastic Actuators," in *2022 IEEE 17th International Conference on Advanced Motion Control (AMC)*, Feb. 2022, pp. 18–23. doi: 10.1109/AMC51637.2022.9729257.

[35] S. Li, J. Li, G. Tian, and H. Shang, "Stiffness Adjustment for a Single-Link Robot Arm Driven by Series Elastic Actuator in Muscle Training," *IEEE Access*, vol. 7, pp. 65029–65039, 2019, doi: 10.1109/ACCESS.2019.2916379.

[36] C. Lee and S. Oh, "Development, Analysis, and Control of Series Elastic Actuator-Driven Robot Leg," *Front. Neurorobotics*, vol. 13, 2019, Accessed: Jul. 05, 2023. [Online]. Available: https://www.frontiersin.org/articles/10.3389/fnbot.2019.00017

[37] B. Soe, "Design and Control of Series Elastic Actuators for Disturbance Rejection," Eng., Stanford University, United States -- California, 2017. Accessed: Jul. 11, 2023. [Online]. Available: https://www.proquest.com/docview/2510268192/abstract/B8EE5DF65B8A4F6APQ/1

[38] T. Lens and O. Von Stryk, *Design and dynamics model of a lightweight series elastic tendon-driven robot arm*. 2013, p. 4518. doi: 10.1109/ICRA.2013.6631218.